IOP Publishing — Journal of Physics: Condensed Matter
J. Phys.: Condens. Matter **20** (2008) 045206 (10pp) doi:10.1088/0953-8984/20/04/045206

Many-body effects in two-dimensional optical spectra of semiconductor quantum dot pairs; time-dependent Hartree–Fock approximation and beyond

R Oszwałdowski[1,2], D Abramavicius[1] and S Mukamel[1]

[1] Department of Chemistry, University of California, Irvine, CA 92697, USA
[2] Instytut Fizyki UMK, Grudziądzka 5/7, 87-100 Toruń, Poland

E-mail: rosz@fizyka.umk.pl

Received 28 September 2007, in final form 29 November 2007
Published 8 January 2008
Online at stacks.iop.org/JPhysCM/20/045206

Abstract
We calculate coherent, third-order, nonlinear spectra of a pair of quantum dots by solving the nonlinear exciton equations, which include relevant single-exciton and two-exciton variables. The signals carry direct information on exciton dynamics and correlations. Spectra calculated with the time-dependent Hartree–Fock approximation, where the two-exciton variables are factorized, miss some important features, attributed to correlated electron–hole pairs.

(Some figures in this article are in colour only in the electronic version)

1. Introduction

The study of optical excitations in quantum dots has been a major focus of semiconductor physics over the past decade [1, 2]. Their unique physical properties have drawn attention from diverse fields such as laser physics [3, 4], quantum information [5, 6], and medical diagnostics [7, 8]. Precise growth of multiple quantum dots is possible [9], pairs of dots with ~10 nm spacing were grown on a semiconductor substrate [10]. Their optical properties are described in terms of single and multiple excitons [11–14]. Correlations between these quasiparticles determine the nonlinear optical response [15].

An advanced class of four-wave-mixing techniques, known as two-dimensional spectroscopy, has become an important tool for studying both vibrational and electronic coherences [16–18] in a broad range of systems such as liquid methane [19], rubidium vapor [20], and light-harvesting complexes [21]. Recently, these powerful methods have been applied successfully to semiconductor quantum wells [22–24] and quantum dots (QDs) [25]. Two-dimensional experimental spectra display a variety of features, that can be directly linked to coherences created by interaction with light on the femtosecond time scale.

In this paper we compute two-dimensional correlation spectra of coupled QDs using a simple tight-binding Hamiltonian [26]. Owing to Coulomb interactions and the non-bosonic nature of excitons, the Heisenberg equations of motion for polarization couple to higher dynamical variables, which opens an infinite hierarchy of coupled quantities. We truncate this hierarchy at two levels [27]. The first, derived within the nonlinear exciton equations (also known as dynamics controlled truncation) scheme, retains the four-point variables (Y) required to describe signals to third order in the field. This approach yields exact many-body wavefunctions and levels for the pair-conserving Hamiltonian used in this paper. The second truncation scheme, based on time-dependent Hartree–Fock (THDF) approximation, neglects correlations between excitons by factorizing the Y variables and uses only two-point quantities. It is widely employed owing to its simplicity and smaller computational requirements [14].

The resulting equations of motion can be solved by direct numerical integration [24, 28, 29]. In this paper, however, in order to gain a better insight into the nature of the optical response, we use Green's functions to solve the equations formally and derive closed expressions for the third-order response functions. We compare the TDHF response functions with the nonlinear exciton equation (NEE) expressions reported earlier [30, 31]. These formulas allow us to predict some general features of the two-dimensional spectra before performing numerical calculations. We next present the results of our NEE and TDHF calculations for two techniques used in two-dimensional spectroscopy. We show that the TDHF response functions miss some important features of the full NEE response.

The outline of the paper is as follows: in section 2 we define the two-band electron–hole Hamiltonian used to describe quantum dot systems. We also give the Heisenberg equations of motion and the TDHF factorization. In section 3 we compare the TDHF response functions to their NEE counterparts. Numerical results obtained from both expressions are presented in section 4, and a general discussion follows in section 5.

2. The NEE and the TDHF equations of motion for a two-band Hamiltonian

We start with a tight-binding, two-band Hamiltonian, where each site at a position R represents one QD with two single-electron levels

$$H = H_0 + H_{\mathrm{C}} + H_{\mathrm{L}}. \tag{1}$$

The one-particle part H_0, which accounts for electron and hole hopping between the QDs, can be written in the form of equation (B1) of [32]

$$H_0 = \sum_{m_1,n_1} t^{(1)}_{m_1,n_1} c^\dagger_{m_1} c_{n_1} + \sum_{m_2,n_2} t^{(2)}_{m_2,n_2} d^\dagger_{m_2} d_{n_2},$$

where the indices are $m_1 = (R_{\mathrm{e}_1}, \sigma_{\mathrm{e}_1})$, $n_1 = (R_{\mathrm{e}_2}, \sigma_{\mathrm{e}_2})$, $m_2 = (R_{\mathrm{h}_1}, \sigma_{\mathrm{h}_1})$, $n_2 = (R_{\mathrm{h}_2}, \sigma_{\mathrm{h}_2})$, σ is the spin projection and the Fermi operators c (d) annihilate electrons (holes). R_{e} (R_{h}) is the electron (hole) position.

The many-body part H_{C} describes monopole–monopole Coulomb interactions

$$\begin{aligned} H_{\mathrm{C}} = &- \sum_{m_1,m_2} V^{\mathrm{eh}}_{m_1 m_2} c^\dagger_{m_1} d^\dagger_{m_2} d_{m_2} c_{m_1} \\ &+ \tfrac{1}{2} \sum_{m_1,n_1} V^{\mathrm{ee}}_{m_1 n_1} c^\dagger_{m_1} c^\dagger_{n_1} c_{n_1} c_{m_1} + \tfrac{1}{2} \sum_{m_2,n_2} V^{\mathrm{hh}}_{m_2 n_2} d^\dagger_{m_2} d^\dagger_{n_2} d_{n_2} d_{m_2}. \end{aligned} \tag{2}$$

This simple model, which neglects some Coulomb (exchange and four-point) integrals is known to describe correctly the influence of many-body correlations on optical spectra of semiconductors [26].

We treat the interaction with light in the dipole approximation:

$$\begin{aligned} \hat{H}_L &= -\boldsymbol{E}(t) \cdot \hat{\boldsymbol{P}} \\ &= -\boldsymbol{E}(t) \cdot \left(\sum_{m_1,m_2} \boldsymbol{\mu}^*_{m_1 m_2} c^\dagger_{m_1} d^\dagger_{m_2} + \boldsymbol{\mu}_{m_1 m_2} d_{m_2} c_{m_1} \right), \end{aligned}$$

where $\boldsymbol{\mu}$ are the on-site dipole matrix elements and $\boldsymbol{E}(t) = \boldsymbol{E}^+(t)\exp(\mathrm{i}\boldsymbol{kr} - \mathrm{i}\omega t) + \boldsymbol{E}^-(t)\exp(-\mathrm{i}\boldsymbol{kr} + \mathrm{i}\omega t)$.

Electron–hole (e–h) pairs are responsible for the fundamental resonances with energies close to the band-gap. We therefore follow the quasiparticle approach of [32], where the Hamiltonian (1) was recast in terms of electron–hole operators $\hat{B}_n = d_{n_2} c_{n_1}$. Next, the Heisenberg equations of motion (EOM) for the expectation values $B_n = \langle \hat{B}_n \rangle$ were derived to obtain the polarization $\boldsymbol{P}$. The hierarchy of multi-point quantities was truncated by retaining only the two-point $B_n = \langle d_{n_2} c_{n_1} \rangle$ and the four-point $Y_{mn} = \langle d_{m_2} c_{m_1} d_{n_2} c_{n_1} \rangle = \langle B_m B_n \rangle$ [33]. The resulting NEE, expanded in orders of the laser field $E(t)$ (indicated by superscripts) are

$$\begin{aligned} \mathrm{i}\frac{\mathrm{d}B^{(1)}_m}{\mathrm{d}t} &= \sum_n h_{mn} B^{(1)}_n - \boldsymbol{\mu}^*_m \boldsymbol{E}^+(t), \\ \mathrm{i}\frac{\mathrm{d}Y^{(2)}_{mn}}{\mathrm{d}t} &= \sum_{k,l} h^{(Y)}_{mn,kl} Y^{(2)}_{kl} - \boldsymbol{E}^+(t)(B^{(1)}_n \boldsymbol{\mu}^*_m \\ &\quad + B^{(1)}_m \boldsymbol{\mu}^*_n) + 2\boldsymbol{E}^+(t) \sum_{k,l} \mathcal{P}_{mnkl} B^{(1)}_k \boldsymbol{\mu}^*_l, \\ \mathrm{i}\frac{\mathrm{d}B^{(3)}_m}{\mathrm{d}t} &= \sum_n h_{mn} B^{(3)}_m + \sum_{n,k,l} \widetilde{V}_{mnkl} B^{(1)*}_n Y^{(2)}_{kl} \\ &\quad + 2\boldsymbol{E}^+(t) \sum_{n,p,q} \mathcal{P}_{mnpq} B^{(1)*}_n B^{(1)}_q \boldsymbol{\mu}^*_p. \end{aligned} \tag{3}$$

h_{mn} is the Hamiltonian $H_0 + H_{\mathrm{C}}$ projected on singly excited states. The m, n indices run over all $(2N)^2$ possible e–h pairs, where N is the number of sites (QDs). The $(2N)^4 \times (2N)^4$ tetradic matrices $h^{(Y)}_{mn,kl}$ and $\widetilde{V}_{mnkl}$ are defined [32] by the parameters appearing in H_0 and H_{C}. We use the rotating wave approximation and set $\hbar = 1$. Dephasing will be added phenomenologically in the final formulas.

The two source terms in the equation for $B^{(3)}_m$ represent the Coulomb interaction and Pauli blocking, respectively. The operator $\mathcal{P}$, equation (A.1), represents the commutation rules of the $\hat{B}_n$ operators

$$\mathcal{P}_{mnpq} = \tfrac{1}{2}\left(\delta_{m_1 q_1} \delta_{n_1 p_1} \delta_{m_2 p_2} \delta_{n_2 q_2} + \delta_{m_1 p_1} \delta_{n_1 q_1} \delta_{m_2 q_2} \delta_{n_2 p_2} \right). \tag{4}$$

The TDHF approximation to the NEE is introduced by factorizing the two-exciton variable $Y_{mn} \simeq \langle d_{m_2} c_{m_1} \rangle \langle d_{n_2} c_{n_1} \rangle - \langle d_{m_2} c_{n_1} \rangle \langle d_{n_2} c_{m_1} \rangle$ [34]. In terms of the exciton variables it reads

$$Y_{mn} = \langle B_m B_n \rangle \simeq \sum_{p,q} (\mathbb{I} - \mathcal{P})_{mnpq} B_p B_q. \tag{5}$$

Using equation (5) we obtain the following TDHF equations of motion

$$\begin{aligned} \mathrm{i}\frac{\mathrm{d}B^{(1)}_m}{\mathrm{d}t} &= \sum_n h_{mn} B^{(1)}_n - \boldsymbol{\mu}^*_m \boldsymbol{E}^+(t), \\ \mathrm{i}\frac{\mathrm{d}B^{(3)}_m}{\mathrm{d}t} &= \sum_n h_{mn} B^{(3)}_m \\ &\quad + \sum_{n,k,l} \sum_{p,q} \widetilde{V}_{mnkl} (\mathbb{I} - \mathcal{P})_{klpq} B^{(1)*}_n B^{(1)}_p B^{(1)}_q \\ &\quad + 2\boldsymbol{E}^+(t) \sum_{n,p,q} \mathcal{P}_{mnpq} B^{(1)*}_n B^{(1)}_q \boldsymbol{\mu}^*_p. \end{aligned} \tag{6}$$

The factorization (5) neglects the correlated part of $\langle B_m B_n \rangle$. Thus equations (6) are an approximation to equations (3).

3. Two-dimensional signals

The EOM for both factorizations, equations (3) or (6), can be formally solved using Green's functions to obtain

$$P_{\nu_4}(\tau_4) = \int_0^{+\infty} \mathrm{d}t_3\,\mathrm{d}t_2\,\mathrm{d}t_1 S^{\nu_4\nu_3\nu_2\nu_1}(t_3,t_2,t_1) \times E_{\nu_3}(\tau_4 - t_3)E_{\nu_2}(\tau_4 - t_2 - t_3)E_{\nu_1}(\tau_4 - t_1 - t_2 - t_3), \quad (7)$$

where $P(\tau_4)$ is the polarization at time τ_4, the tensor $S^{\nu_4\nu_3\nu_2\nu_1}$ is the response function, t_1, t_2, t_3 are delays between light pulses and ν_i are Cartesian components of the pulses' polarizations. [30] We focus on three types of four-wave-mixing signals generated along the phase matching directions $\boldsymbol{k}_{\rm I} = -\boldsymbol{k}_1 + \boldsymbol{k}_2 + \boldsymbol{k}_3$, $\boldsymbol{k}_{\rm II} = \boldsymbol{k}_1 - \boldsymbol{k}_2 + \boldsymbol{k}_3$ and $\boldsymbol{k}_{\rm III} = \boldsymbol{k}_1 + \boldsymbol{k}_2 - \boldsymbol{k}_3$, where $\boldsymbol{k}_1$, $\boldsymbol{k}_2$ and $\boldsymbol{k}_3$ are the wavevectors of the three incoming pulses. A useful visualization of the information carried by the response function $S(t_3, t_2, t_1)$ is obtained by Fourier transforming it with respect to two of the time delays. We choose them to be t_1 and t_3 for the $\boldsymbol{k}_{\rm I}$ and $\boldsymbol{k}_{\rm II}$ techniques, while for $\boldsymbol{k}_{\rm III}$ we take t_2 and t_3 [35]. We denote the frequency conjugate to t_j by Ω_j.

Both NEE and TDHF response functions S are expressed using the tetradic, $(2N)^4 \times (2N)^4$ exciton scattering matrix Γ. For the NEE it is defined as

$$\Gamma^{\rm NEE}(\omega) = \left[\mathbb{I} - \widetilde{V}G(\omega)\right]^{-1}\widetilde{V}G(\omega)\,(\mathbb{I} - \mathcal{P}) \times G(\omega)^{-1} - \mathcal{P}G(\omega)^{-1}, \quad (8)$$

while for the TDHF

$$\Gamma^{\rm TDHF}(\omega) = \widetilde{V}\,(\mathbb{I} - \mathcal{P}) - \mathcal{P}G(\omega)^{-1}, \quad (9)$$

where $G_{e_2e_1}(\omega) = (\omega - \varepsilon_{e_2} - \varepsilon_{e_1} + \mathrm{i}\gamma_{e_2} + \mathrm{i}\gamma_{e_1})^{-1}$ (cf[3]).

Below we give the response functions for the three techniques. We introduce decoherence effects by adding dephasing rates $\mathrm{i}\gamma_{\rm e}$ to single-exciton energies $\varepsilon_{\rm e}$. This is adequate in many physical situations [31].

The response function for $\boldsymbol{k}_{\rm I}$ is:

$$S_{\rm I}^{\nu_4\nu_3\nu_2\nu_1}(\Omega_3, t_2, \Omega_1) = 2\mathrm{i}\sum_{e_1\ldots e_4}\mu_{e_1}^{\nu_1}\mu_{e_2}^{\nu_2 *}\mu_{e_3}^{\nu_3 *}\mu_{e_4}^{\nu_4} \times I_{e_1}^*(t_2)\,I_{e_2}(t_2)\,I_{e_1}^*(-\Omega_1)\,I_{e_4}(\Omega_3) \times \Gamma_{e_4e_1e_2e_3}\left(\Omega_3 + \varepsilon_{e_1} + \mathrm{i}\gamma_{e_1}\right)G_{e_3e_2}\left(\Omega_3 + \varepsilon_{e_1} + \mathrm{i}\gamma_{e_1}\right), \quad (10)$$

where $I_{\rm e}(\omega) = (\omega - \varepsilon_{\rm e} + \mathrm{i}\gamma_{\rm e})^{-1}$ and $I_{\rm e}(t) = -\mathrm{i}\theta(t)\exp(-\mathrm{i}\varepsilon_{\rm e}t - \gamma_{\rm e}t)$.

For $\boldsymbol{k}_{\rm II}$ we find

$$S_{\rm II}^{\nu_4\nu_3\nu_2\nu_1}(\Omega_3, t_2, \Omega_1) = -2\mathrm{i}\sum_{e_1\ldots e_4}\mu_{e_1}^{\nu_1 *}\mu_{e_2}^{\nu_2}\mu_{e_3}^{\nu_3 *}\mu_{e_4}^{\nu_4} \times I_{e_2}^*(t_2)I_{e_1}(t_2)I_{e_1}(\Omega_1)I_{e_4}(\Omega_3) \times \Gamma_{e_4e_2e_3e_1}(\Omega_3 + \varepsilon_{e_2} + \mathrm{i}\gamma_{e_2})G_{e_3e_1}(\Omega_3 + \varepsilon_{e_2} + \mathrm{i}\gamma_{e_2}). \quad (11)$$

Finally, the $\boldsymbol{k}_{\rm III}$ signal is given by

$$S_{\rm III}^{\nu_4\nu_3\nu_2\nu_1}(\Omega_3, \Omega_2, t_1) = 2\sum_{e_1\ldots e_4}\mu_{e_1}^{\nu_1 *}\mu_{e_2}^{\nu_2 *}\mu_{e_3}^{\nu_3}\mu_{e_4}^{\nu_4} \times I_{e_1}(t_1)\,I_{e_4}(\Omega_3)\,I_{e_3}^*(\Omega_2 - \Omega_3) \times \{\Gamma_{e_4e_3e_2e_1}(\Omega_3 + \varepsilon_{e_3} + \mathrm{i}\gamma_{e_3})G_{e_2e_1}(\Omega_3 + \varepsilon_{e_3} + \mathrm{i}\gamma_{e_3}) - \Gamma_{e_4e_3e_2e_1}(\Omega_2)G_{e_2e_1}(\Omega_2)\}. \quad (12)$$

[3] In [31] we used the symbol $\mathcal{G}_0$ instead of G to distinguish this quantity from other Green's functions.

The term $\mathcal{P}G^{-1}$ in equations (8) and (9), which arises from Pauli blocking (exciton statistics), cancels out in equation (12). Such cancellation does not occur for the $\boldsymbol{k}_{\rm I}$ or $\boldsymbol{k}_{\rm II}$ techniques. This important difference between the techniques will be discussed in section 5.

The TDHF response function for $\boldsymbol{k}_{\rm III}$ is more easily analyzed when transformed to

$$S_{\rm III,TDHF}^{\nu_4\nu_3\nu_2\nu_1}(\Omega_3, \Omega_2, t_1) = 2\sum_{e_1\ldots e_4}\mu_{e_1}^{\nu_1 *}\mu_{e_2}^{\nu_2 *}\mu_{e_3}^{\nu_3}\mu_{e_4}^{\nu_4}I_{e_1}(t_1)G_{e_2e_1}(\Omega_2) \times I_{e_4}(\Omega_3)G_{e_2e_1}\left(\Omega_3 + \varepsilon_{e_3} + \mathrm{i}\gamma_{e_3}\right)\left[\widetilde{V}\,(\mathbb{I} - \mathcal{P})\right]_{e_4e_3e_2e_1}. \quad (13)$$

Equations (10)–(12) are obtained after symmetrizing $\widetilde{V}$ with respect to permutation of the two last indices, as shown in appendix B.

4. Numerical simulations

We first describe briefly some general features of $\boldsymbol{k}_{\rm I}$ and $\boldsymbol{k}_{\rm III}$ spectra ($\boldsymbol{k}_{\rm II}$ is qualitatively similar to $\boldsymbol{k}_{\rm I}$ and will not be further considered). Next we explain the choice of the QD parameters and present the numerical results.

From equation (10) for $\boldsymbol{k}_{\rm I}$, we see that for both NEE and TDHF, the Ω_1 coordinate of any peak corresponds to minus single-exciton energy, $\Omega_1 \simeq -\varepsilon_{e_1}$. For TDHF the Ω_3 resonances (i.e. small values of the denominators) appear at either $\Omega_3 \simeq \varepsilon_{e_4}$ or $\Omega_3 \simeq (\varepsilon_{e_2} + \varepsilon_{e_3}) - \varepsilon_{e_1}$. Peaks in the absolute value of the response function only exist for $\mu_{e_1}\mu_{e_4} \neq 0$ in the former case, and for $\mu_{e_1}\mu_{e_2}\mu_{e_3} \neq 0$ in the latter case. For the TDHF $\boldsymbol{k}_{\rm III}$ response function, equation (13), a resonance along the Ω_2 axis appears if $\Omega_2 \simeq \varepsilon_{e_1} + \varepsilon_{e_2}$ and $\mu_{e_1}\mu_{e_2} \neq 0$. Along Ω_3, it has the same resonances as for $\boldsymbol{k}_{\rm I}$.

This analysis allows us to predict the peak positions for the TDHF, but not for the NEE, where the scattering matrix (8) has a complicated frequency dependence. Thus we shall analyze the NEE response using sum-over-states (SOS) expressions [31, 36, 44], which allow an easy classification of spectral features. In most cases, however, they are not useful for *calculating* the spectra, since the SOS approach requires the calculation of doubly excited energies and wavefunctions [37]. This is avoided by using the NEE or TDHF approaches.

We use a set of parameters for InGaAs quantum dots, where the valence (conduction) band is constructed of p (s) orbitals. The initially occupied single-particle level of each QD is derived from bulk heavy-hole states with angular momentum quantum numbers $|J, M\rangle$ equal to $|\frac{3}{2}, \frac{3}{2}\rangle$ or $|\frac{3}{2}, -\frac{3}{2}\rangle$. The empty level is derived from conduction band states $|\frac{1}{2}, \frac{1}{2}\rangle$, $|\frac{1}{2}, -\frac{1}{2}\rangle$. The on-site energies for electrons ($\epsilon_{\rm e}$) and holes ($\epsilon_{\rm h}$) in H_0 are defined by the band-gap and quantum confinement. They can be extracted from pseudopotential calculations [38]. To simplify the analysis of the spectra, we omit these energies, they can be simply reintroduced by shifting the Ω_1 (Ω_3) values up (down) by $E_{\rm g} = \epsilon_{\rm e} + \epsilon_{\rm h}$ in the results for $\boldsymbol{k}_{\rm I}$ (figures 1 and 2). For $\boldsymbol{k}_{\rm III}$ (figures 3–5) the Ω_2 (Ω_3) values must be shifted up by $2E_{\rm g}$ ($E_{\rm g}$). We assume that only on-site (single QD) dipole moments are non-zero $\mu_{R_{\rm e},\sigma_{\rm e};R_{\rm h},\sigma_{\rm h}} \sim \delta_{R_{\rm e},R_{\rm h}}$. For

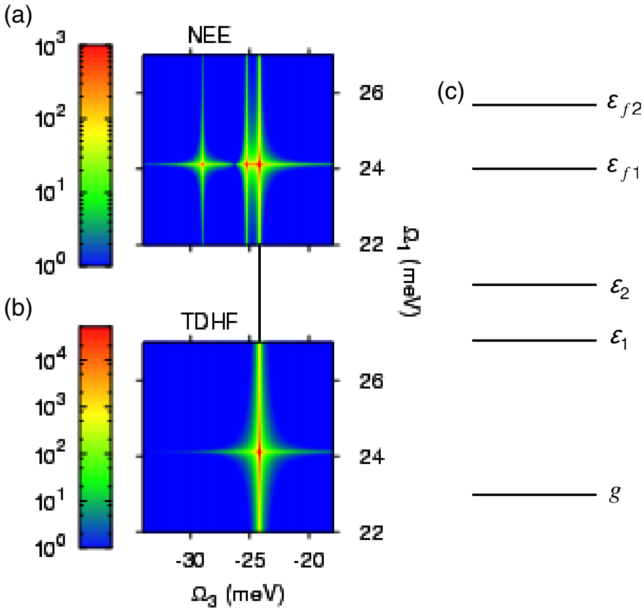

Figure 1. Absolute value of NEE (panel (a)) and TDHF (panel (b)) response functions for the $\boldsymbol{k}_{\rm I}$ technique obtained for system W of two weakly coupled quantum dots and $xxxx$ polarization. The axes Ω_3 and Ω_1 are Fourier transforms of the delays t_3 and t_1 between laser pulses. The vertical line joining the panels indicates the diagonal peak at $(\Omega_3, \Omega_1) = (-V(0), V(0))$, which is common to both spectra. Panel (c) many-particle levels of system W; the ground, single-exciton, and double-exciton levels are marked by g, ε_i and $\varepsilon_{\rm f_i}$, respectively.

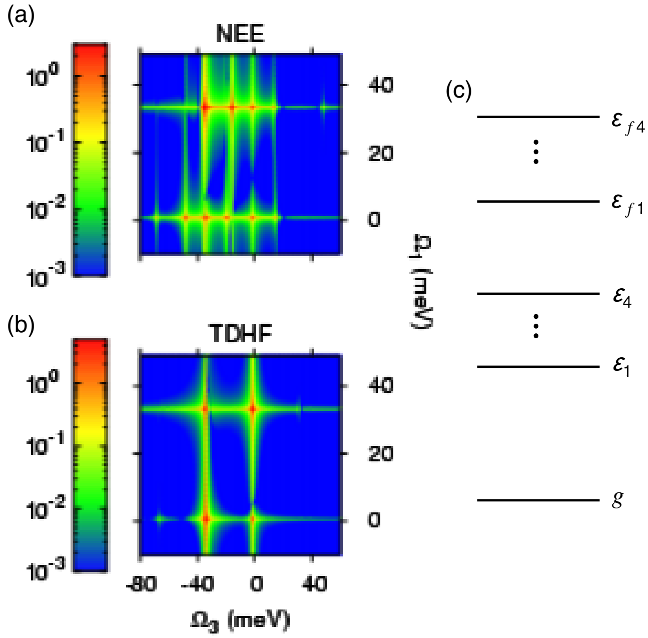

Figure 2. Absolute value of NEE (panel (a)) and TDHF (panel (b)) response functions for the $\boldsymbol{k}_{\rm I}$ technique obtained for system S of two strongly coupled quantum dots and $xxxx$ polarization. The two horizontal rows of peaks correspond to two single-exciton bright states at -33 and -0.5 meV. Panel (c) many-particle levels; the ground, single-exciton and double-exciton levels are marked by g, ε_i and ε_{f_i} respectively.

excitations from the $|\frac{3}{2}, \frac{3}{2}\rangle$ level we assume $\boldsymbol{\mu}_{\sigma_{\rm e},\uparrow} = \frac{1}{\sqrt{2}}\mu_0(\hat{x} + {\rm i}\hat{y})\delta_{\sigma_{\rm e},\uparrow}$, while for excitations from the $|\frac{3}{2}, -\frac{3}{2}\rangle$ level: $\mu_{\sigma_{\rm e},\downarrow} = \frac{1}{\sqrt{2}}\mu_0(\hat{x} - {\rm i}\hat{y})\delta_{\sigma_{\rm e},\downarrow}$ [39].

All parameters of $H_{\rm C}$ depend on the distance between two sites, e.g., $V^{\rm eh}_{m_1 n_1} = V^{\rm eh}(R_{\rm e_1} - R_{\rm e_2})$. We extracted $V^{\rm eh}(0)$ (e–h interaction on the same dot) and $V^{\rm eh}(1)$ (e–h interaction between two QDs) values from the transition energies calculated for double QDs, which agree qualitatively with emission spectra of pairs of InAs/GaAs QDs with varying distances [40].

For a single InGaAs QD the $V^{\rm ee}(0)$ and $V^{\rm hh}(0)$ are approximately equal to $V^{\rm eh}(0)$ [41]. We assume that this approximate equality holds also for $V(1)$ for pairs of coupled QDs. We write $V^{\rm ee}(i) = V^{\rm hh}(i) = aV^{\rm eh}(i)$ with $i = 0, 1$, where a defines the asymmetry of the interactions. For $a = 1$ (symmetric interactions) a single QD system described by $H_0 + H_{\rm C}$ becomes harmonic, in the sense that the doubly excited state's energy $\varepsilon_{\rm f}$ is exactly twice the singly excited state $\varepsilon_{\rm e}$ energy, $\varepsilon_{\rm f} = 2\varepsilon_{\rm e}$ [42].

We used two QD systems in our simulations. The first (system W), consists of two weakly coupled ($d \sim 10$ nm) quantum dots with the interaction asymmetry $a = 0.9$. For this spacing the hopping t can be neglected, while the dots are still coupled by Coulomb interaction. We use $V(0) \simeq 24$ and $V(1) \simeq 5$ meV.

In the second system (S) we assume an inter-dot spacing of 5 nm. The dots are thus strongly coupled with a hopping $t \simeq 7$ meV, assumed to be the same for electrons and holes. The Coulomb interactions are taken to be symmetric, $a = 1$, with $V(0) \simeq 24$ and $V(1) \simeq 10$ meV.

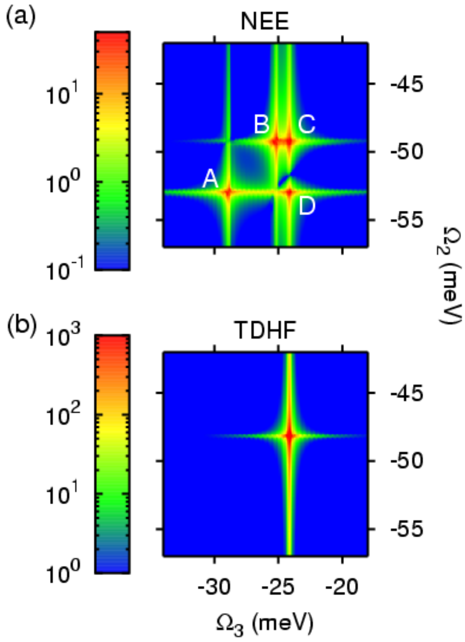

Figure 3. Absolute value of NEE and TDHF response functions for the $\boldsymbol{k}_{\rm III}$ technique obtained for system W of two weakly coupled quantum dots and $xxxx$ polarization. Peaks A, B, C and D are at $(\varepsilon_{\rm f_1} - \varepsilon_1, \varepsilon_{\rm f_1})$, $(\varepsilon_{\rm f_2} - \varepsilon_1, \varepsilon_{\rm f_2})$, $(\varepsilon_1, \varepsilon_{\rm f_2})$, and $(\varepsilon_1, \varepsilon_{\rm f_1})$, respectively.

All wavefunctions can be grouped according to the spins of electrons and holes: (σ_e, σ_h) for the single excitations and $(\Sigma_e = \sigma_{e_1} + \sigma_{e_2}, \Sigma_h = \sigma_{h_1} + \sigma_{h_2})$ for double excitations, where $\sigma_{e,h} = \pm 1$. Since the hoppings $t^{(1,2)}$ are spin diagonal, subspaces with different (σ_e, σ_h) or (Σ_e, Σ_h) are not coupled to each other. Single-exciton states $(\sigma_e = \pm 1, \sigma_h = \pm 1)$ are at least fourfold degenerate. Wavefunctions constructed in the $(\sigma_e, \sigma_h) = (+1, -1), (-1, +1)$ and $(\Sigma_e, \Sigma_h) = (0, \pm 2), (\pm 2, 0), (2, -2), (-2, 2)$ subspaces are optically forbidden. The subspaces $(2, 2)$ and $(-2, -2)$ are one-dimensional, with states formed by placing one exciton on each dot. The exact eigenenergy of these states is $-2V(0)$ and does not depend on the hopping. The $(0, 0)$ subspace contains 16 wavefunctions, coupled by hopping in the case of system S.

We set $t_2 = 0$ $(t_1 = 0)$ for the $\boldsymbol{k}_{\mathrm{I}}$ $(\boldsymbol{k}_{\mathrm{III}})$ techniques. We use a small dephasing rate $(\gamma \sim 10^{-3}$ meV) to obtain high-resolution spectra.

4.1. The $\boldsymbol{k}_I$ technique

To analyze the TDHF spectra we use equations (10) and (9). For the NEE we use the SOS formula [31]

$$S_{\mathrm{I}}^{\nu_4\nu_3\nu_2\nu_1}(\Omega_3, t_2 = 0, \Omega_1) = \mathrm{i} \sum_{\mathrm{e,e'}} \frac{\mu_{\mathrm{ge'}}^{\nu_1}}{\Omega_1 + \varepsilon_{\mathrm{e'}} + \mathrm{i}\gamma_{\mathrm{e'g}}} \times \left[\sum_{\mathrm{f}} \frac{\mu_{\mathrm{eg}}^{\nu_2} \mu_{\mathrm{fe}}^{\nu_3} \mu_{\mathrm{e'f}}^{\nu_4}}{\Omega_3 - (\varepsilon_{\mathrm{f}} - \varepsilon_{\mathrm{e'}}) + \mathrm{i}\gamma_{\mathrm{fe'}}} - \frac{\mu_{\mathrm{ge}}^{\nu_4} \left(\mu_{\mathrm{eg}}^{\nu_2} \mu_{\mathrm{e'g}}^{\nu_3} + \mu_{\mathrm{e'g}}^{\nu_2} \mu_{\mathrm{eg}}^{\nu_3} \right)}{\Omega_3 - \varepsilon_{\mathrm{e}} + \mathrm{i}\gamma_{\mathrm{eg}}} \right], \tag{14}$$

where g stands for the ground state with zero energy, e, e′ denote singly excited states and f runs over the doubly excited manifold. γ_{fe} and γ_{eg} are dephasing rates of the corresponding density matrix elements.

Equation (14) predicts two types of resonances along the Ω_3 axis. The first, $\Omega_3 \simeq \varepsilon_{\mathrm{e}}$, is analogous to the TDHF response. The second, $\Omega_3 \simeq \varepsilon_{\mathrm{f}} - \varepsilon_{\mathrm{e'}}$, coincides with its TDHF counterpart only for systems where the doubly excited energies are sums of the singly excited ones.

System W has two single-exciton levels, bright (1) and dark (2). The former, with both quasiparticles on one dot, has energy $\varepsilon_1 = -V(0)$. The latter corresponds to electron and hole on different QDs, and $\varepsilon_2 = -V(1)$. There are two optically allowed double-exciton levels (figure 1(c)); f_1 (f_2) with two excitons on the same (different) dot. Their energies are $-4V^{\mathrm{eh}}(0) + V^{\mathrm{ee}}(0) + V^{\mathrm{hh}}(0)$ and $-2V^{\mathrm{eh}}(0) - 2V^{\mathrm{eh}}(1) + V^{\mathrm{ee}}(1) + V^{\mathrm{hh}}(1)$, respectively.

For this model, the TDHF response has a single peak at $(\Omega_3, \Omega_1) = (\varepsilon_1, -\varepsilon_1)$, (figure 1(b)), as follows from our above analysis. As predicted by equation (14), the NEE spectra reveal, in addition to the diagonal $(\varepsilon_1, -\varepsilon_1)$ feature, two peaks at $\Omega_3 \simeq \varepsilon_{\mathrm{f}_1} - \varepsilon_1 \simeq -29$ meV (both excitons on the same QD) and $\Omega_3 \simeq \varepsilon_{\mathrm{f}_2} - \varepsilon_1 \simeq -25$ meV (each exciton on a different QD). These peaks are below the diagonal one with respect to the Ω_3 axis, because $a = 0.9$ implies a reduced electron–electron and hole–hole repulsion as compared to electron–hole attraction. For $a > 1$ (not shown) the repulsions prevail and the two double-exciton peaks appear above the single-exciton one, this corresponds to unbound biexciton in semiconductor bulk and quantum wells. This regime can be accessed in the type-II QDs, where electrons are spatially separated from holes [43]. For $a = 1.0$, $\varepsilon_{\mathrm{f}_1} = \varepsilon_{\mathrm{f}_2} = 2\varepsilon_1$ and the NEE response collapses to the diagonal peak seen in the TDHF response.

System S has four single-exciton levels (figure 2(c)), $\varepsilon_1 = -33$, $\varepsilon_2 = -24$, $\varepsilon_3 = -10$, and $\varepsilon_4 = -0.5$ meV, where levels 2 and 3 are dark. Both TDHF and NEE response functions are resonant at $\Omega_1 \simeq -\varepsilon_{1,4}$. The possible resonances for the TDHF can appear at $\Omega_3 \simeq \varepsilon_1, \varepsilon_4, 2\varepsilon_4 - \varepsilon_1$ and $2\varepsilon_1 - \varepsilon_4$. Some pairs of these (Ω_3, Ω_1) values do not correspond to peaks in the spectra. For example taking $\Omega_1 \simeq -\varepsilon_1$ (upper row in figure 2(b)), there can be no peak at $\Omega_3 \simeq 2\varepsilon_1 - \varepsilon_4$, as evident from equations (9) and (10).

Each row in the NEE spectrum contains more peaks than for the TDHF (figure 2(a)). To assign the peaks using equation (14) one needs to know the number of optically allowed doubly excited states along with their energies. This information is obtained more directly from the $\boldsymbol{k}_{\mathrm{III}}$ spectra, which we present next.

4.2. The $\boldsymbol{k}_{III}$ technique

The differences between the NEE and the TDHF response are more pronounced for the $\boldsymbol{k}_{\mathrm{III}}$ technique. The TDHF response is given by equation (13), while the NEE one can be conveniently analyzed with the help of the SOS formula

$$S_{\mathrm{III}}^{\nu_4\nu_3\nu_2\nu_1}(\Omega_3, \Omega_2, t_1 = 0) = \mathrm{i} \sum_{\mathrm{e,e',f}} \frac{\mu_{\mathrm{eg}}^{\nu_1} \mu_{\mathrm{fe}}^{\nu_2}}{\Omega_2 - \varepsilon_{\mathrm{f}} + \mathrm{i}\gamma_{\mathrm{fg}}} \times \left[\frac{\mu_{\mathrm{ge'}}^{\nu_4} \mu_{\mathrm{e'f}}^{\nu_3}}{\Omega_3 - (\varepsilon_{\mathrm{f}} - \varepsilon_{\mathrm{e'}}) + \mathrm{i}\gamma_{\mathrm{fe'}}} - \frac{\mu_{\mathrm{ge'}}^{\nu_3} \mu_{\mathrm{e'f}}^{\nu_4}}{\Omega_3 - \varepsilon_{\mathrm{e'}} + \mathrm{i}\gamma_{\mathrm{e'g}}} \right]. \tag{15}$$

We present simulations with all pulses either linearly $(xxxx)$ or circularly $(RRRR)$ polarized. Similarly to $\boldsymbol{k}_{\mathrm{I}}$, equation (14), there are the two types of resonances along Ω_3.

The bright single-exciton states of system W give a resonance at $\Omega_2 \simeq 2\varepsilon_1$ for TDHF. Thus there is only one peak in the TDHF spectrum with $(\Omega_3, \Omega_2) = (\varepsilon_1, 2\varepsilon_1) = (-V(0), -2V(0))$, figure 3(b). The NEE calculations reveal two rows of resonances along Ω_2; at $\varepsilon_{\mathrm{f}_1}$ and $\varepsilon_{\mathrm{f}_2}$. The second term in the square brackets of equation (15) gives rise to a resonance analogous to the TDHF; $\Omega_3 \simeq -V(0)$. The condition $\mu_{\mathrm{ge'}} \neq 0$ allows for appearance of two peaks: $(\Omega_3, \Omega_2) = (\varepsilon_1, \varepsilon_{\mathrm{f}_i})$, $i = 1, 2$. The first term in equation (15) leads to resonances at $(\Omega_3, \Omega_2) = (\varepsilon_{\mathrm{f}_i} - \varepsilon_1, \varepsilon_{\mathrm{f}_i})$. The calculated NEE spectrum is depicted in figure 3(a).

Employing equation (13) to analyze the TDHF response of system S, we find Ω_2 resonances at $2\varepsilon_1, 2\varepsilon_4$ and $\varepsilon_1 + \varepsilon_4$. Similar to $\boldsymbol{k}_{\mathrm{I}}$, peaks appear only for some of (Ω_3, Ω_2) resonances due to the selection rules, figure 4(b). Two TDHF peaks marked by white arrows can only be revealed by studying the sign of the imaginary or real part of S_{III}. These peaks are masked by features C and D, since the former are given by the $\frac{1}{\Omega_3 - \varepsilon}$ factor (from I_{e_4}), while the latter by the double resonances $\frac{1}{\Omega_3 - \varepsilon} \frac{1}{\Omega_3 + \varepsilon - 2\varepsilon}$ (from $I_{\mathrm{e}_4} G_{\mathrm{e}_2 \mathrm{e}_1}$). The double Ω_3 resonances also

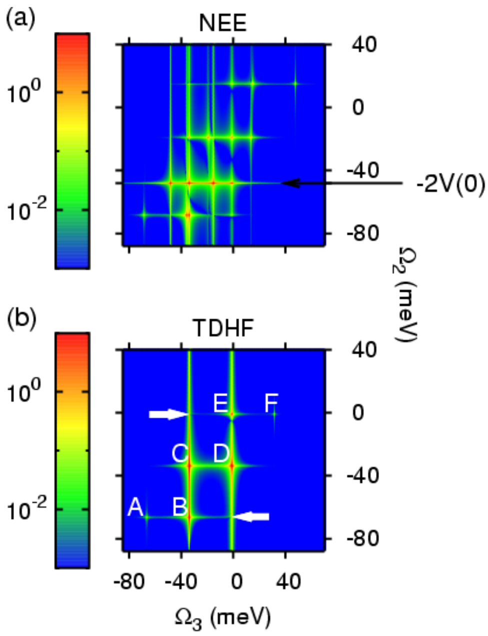

Figure 4. Absolute value of the NEE and TDHF response functions for the $\boldsymbol{k}_{\rm III}$ technique obtained for system S of two strongly coupled quantum dots and $xxxx$ polarization. Panel (a) the arrow indicates peaks corresponding to ε_{f_2}. Panel (b) peaks A, B, C, D, E and F are at $(2\varepsilon_1-\varepsilon_4, 2\varepsilon_1)$, $(\varepsilon_1, 2\varepsilon_1)$, $(\varepsilon_1, \varepsilon_1+\varepsilon_4)$, $(\varepsilon_4, \varepsilon_1+\varepsilon_4)$, $(\varepsilon_4, 2\varepsilon_4)$, and $(2\varepsilon_4-\varepsilon_1, 2\varepsilon_4)$, respectively. White arrows indicate two additional peaks not visible due to their proximity to C and D.

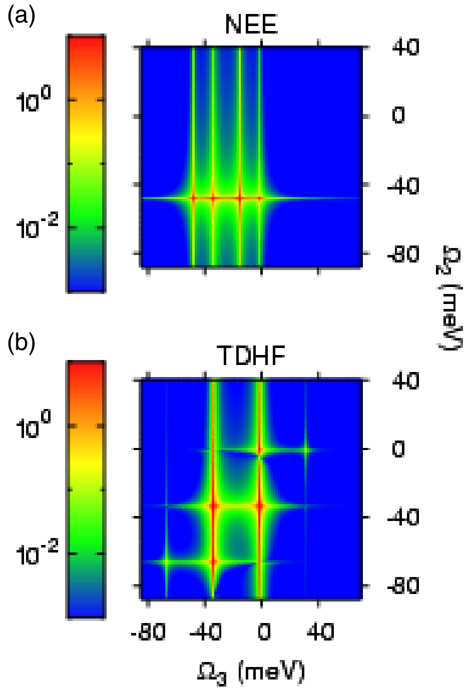

Figure 5. Same as figure 4 but circularly polarized ($RRRR$) pulses.

result in differences between peak width along Ω_3 and along Ω_2, observed for some peaks in the TDHF spectra.

The NEE has more peaks than the TDHF, same as for system W. As seen from figure 4(a), there are four optically allowed doubly excited levels. The energy of the states with $(\Sigma_{\rm e}, \Sigma_{\rm h}) = (2, 2)$ and $(-2, -2)$ is $\varepsilon_{f_2} = -48$ meV. Diagonalization of the $(0, 0)$ block reveals that all states are grouped into 9 levels. States corresponding to 4 of these levels are antisymmetric with respect to exchanging electrons and holes between dots (spatial symmetry) and therefore are optically forbidden. States in a (triply degenerate) spatially symmetrical level are forbidden due to other antisymmetries (either spin flip of all particles or e–h interchange on each QD). There remain four optically allowed levels, one of them is degenerate with the two $(\pm 2, \pm 2)$ states.

Similar to quantum well systems [24], the spins of the particles forming doubly excited states become particularly important, when using circularly polarized light. We calculated the $\boldsymbol{k}_{\rm III}$ response for circularly right-polarized ($RRRR$) pulses, which create spin-up electrons and holes.

For system W only the NEE peak pattern changes with respect to the linearly polarized ($xxxx$) configuration: the peak corresponding to both excitons on one dot is missing due to particle statistics. A similar situation arises for system S (figure 5(b)): only the $(2, 2)$ states can be optically created, so the NEE response shows only one row of resonances, as compared to 4 rows for linear polarization (figure 4(a)). The TDHF response retains the peaks seen in figure 4(a). This shows that, under some conditions, the TDHF spectra may possess more peaks than the NEE ones.

5. Discussion

In section 4 we demonstrated that the NEE and the TDHF spectra are different, both for the $\boldsymbol{k}_{\rm I}$ and $\boldsymbol{k}_{\rm III}$ techniques. To gain further insight into the origin of these differences, let us consider a single QD with two spin-degenerate valence and conduction orbitals. For this simpler system we can derive an explicit expression for the anharmonicity matrix and compare the TDHF and NEE response functions. For the $xxxx$ polarization the TDHF (NEE) $\boldsymbol{k}_{\rm III}$ spectra show one (two) peaks provided $a \neq 1$ [44]. There are two optically allowed single-exciton states with both spins either up or down, and a common energy $\varepsilon_1 = -V^{\rm eh}$, we also assume they have a common decay rate γ_1. The only double-exciton state has energy $\varepsilon_{\rm f} = -4V^{\rm eh} + 2V^{\rm ee} + 2V^{\rm hh}$. We denote the wavefunction of a single-exciton state e_i by ψ_{e_i}. For this system the wavefunction projection on a pair of electron and hole spin orbitals is simply $\psi_{\mathrm{e}_i,\sigma_{\rm e}\sigma_{\rm h}} = \delta_{\sigma_{\rm e}\sigma_{\rm ei}}\delta_{\sigma_{\rm h}\sigma_{{\rm h}i}}$. The transition dipoles are $\mu_{\mathrm{e}_i} = \sum_{\sigma_{\rm e},\sigma_{\rm h}} \psi_{\mathrm{e}_i,\sigma_{\rm e}\sigma_{\rm h}}\mu_{\sigma_{\rm e}\sigma_{\rm h}} = \frac{1}{\sqrt{2}}\mu_0\delta_{\sigma_{{\rm h}i}\sigma_{{\rm e}i}}$. Thus the TDHF response function (13) simplifies to

$$S_{\rm III}^{\rm TDHF}(\Omega_3, \Omega_2, t_1) = \frac{1}{2}\frac{-\mathrm{i}\mu_0^4}{\Omega_2 - 2\varepsilon_1 + 2\mathrm{i}\gamma_1}\frac{1}{(\Omega_3 - \varepsilon_1 + \mathrm{i}\gamma_1)^2} \times \sum_{\mathrm{e}_1\ldots\mathrm{e}_4}\left[\widetilde{V}\left(\mathbb{I} - \mathcal{P}\right)\right]_{\mathrm{e}_4\mathrm{e}_3\mathrm{e}_2\mathrm{e}_1}. \quad (16)$$

Here the summations only run over the two bright states. The anharmonicity matrix $\widetilde{V}$ for this system is diagonal

$$\widetilde{V}_{\mathrm{e}_4\mathrm{e}_3\mathrm{e}_2\mathrm{e}_1} = \widetilde{V}_{\sigma_{\rm e4}\sigma_{\rm h4}\sigma_{\rm e3}\sigma_{\rm h3}\sigma_{\rm e2}\sigma_{\rm h2}\sigma_{\rm e1}\sigma_{\rm h1}} = \left(V^{\rm ee}(0) + V^{\rm hh}(0) - 2V^{\rm eh}(0)\right) \times \delta_{\sigma_{\rm e4}\sigma_{\rm e2}}\delta_{\sigma_{\rm h4}\sigma_{\rm h2}}\delta_{\sigma_{\rm e3}\sigma_{\rm e1}}\delta_{\sigma_{\rm h3}\sigma_{\rm h1}}, \quad (17)$$

which yields $\sum_{\mathrm{e}_1\ldots\mathrm{e}_4}[\widetilde{V}(\mathbb{I}-\mathcal{P})]_{\mathrm{e}_4\mathrm{e}_3\mathrm{e}_2\mathrm{e}_1} = \sum_{\mathrm{e}_1\ldots\mathrm{e}_4}\widetilde{V}_{\mathrm{e}_4\mathrm{e}_3\mathrm{e}_4\mathrm{e}_3}(\mathbb{I} - \mathcal{P})_{\mathrm{e}_4\mathrm{e}_3\mathrm{e}_2\mathrm{e}_1}$. Equation (17) demonstrates that $\widetilde{V}$ measures the deviation of the double-exciton energy from twice the single-exciton energy: $V^{\mathrm{ee}}(0) + V^{\mathrm{hh}}(0) - 2V^{\mathrm{eh}}(0) = -(\varepsilon_{\mathrm{f}} - 2\varepsilon_1)$. Given the form of the transition dipoles (section 4), we can use a common index σ for optically created e–h pairs, and we simplify $(\mathbb{I} - \mathcal{P})_{\sigma_{\mathrm{e4}}\sigma_{\mathrm{h4}}\sigma_{\mathrm{e3}}\sigma_{\mathrm{h3}}\sigma_{\mathrm{e2}}\sigma_{\mathrm{h2}}\sigma_{\mathrm{e1}}\sigma_{\mathrm{h1}}} = \delta_{\sigma_1\sigma_3}\delta_{\sigma_2\sigma_4}(1 - \delta_{\sigma_1\sigma_2})$. We finally obtain

$$
\begin{aligned}
S_{\mathrm{III}}^{\mathrm{TDHF}}(\Omega_3, \Omega_2, t_1) &= \frac{\mathrm{i}}{2}\frac{\mu_0^4}{\Omega_2 - 2\varepsilon_1 + 2\mathrm{i}\gamma_1}\frac{1}{(\Omega_3 - \varepsilon_1 + \mathrm{i}\gamma_1)^2} \\
&\quad \times \sum_{\sigma_1,\sigma_2} (\varepsilon_{\mathrm{f}} - 2\varepsilon_1)\left(1 - \delta_{\sigma_2\sigma_1}\right) \\
&= \frac{\mathrm{i}\mu_0^4}{\Omega_2 - 2\varepsilon_1 + 2\mathrm{i}\gamma_1}\frac{\varepsilon_{\mathrm{f}} - 2\varepsilon_1}{(\Omega_3 - (2\varepsilon_1 - \varepsilon_1) + \mathrm{i}\gamma_1)(\Omega_3 - \varepsilon_1 + \mathrm{i}\gamma_1)}.
\end{aligned} \tag{18}
$$

This can be compared with the NEE result. The exact doubly excited state is given by a direct product of the two single excitations. We then have $\mu_{\mathrm{ge}}\mu_{\mathrm{ef}}\mu_{\mathrm{fe'}}\mu_{\mathrm{e'g}} = \frac{1}{4}\mu_0^4$ and equation (15) becomes

$$
\begin{aligned}
S_{\mathrm{III}}^{\mathrm{NEE}}(\Omega_3, \Omega_2, t_1) &= \frac{\mathrm{i}\mu_0^4}{4}\frac{1}{\Omega_2 - \varepsilon_{\mathrm{f}} + \mathrm{i}\gamma_{\mathrm{fg}}} \\
&\quad \times \sum_{\mathrm{e,e'}} \frac{\varepsilon_{\mathrm{f}} - 2\varepsilon_{\mathrm{e'}} + \mathrm{i}\left(\gamma_{\mathrm{e'g}} - \gamma_{\mathrm{fe'}}\right)}{(\Omega_3 - (\varepsilon_{\mathrm{f}} - \varepsilon_{\mathrm{e'}}) + \mathrm{i}\gamma_{\mathrm{fe'}})\left(\Omega_3 - \varepsilon_{\mathrm{e'}} + \mathrm{i}\gamma_{\mathrm{e'g}}\right)} \\
&= \frac{\mathrm{i}\mu_0^4}{\Omega_2 - \varepsilon_{\mathrm{f}} + \mathrm{i}\gamma_{\mathrm{fg}}}\frac{\varepsilon_{\mathrm{f}} - 2\varepsilon_1 + \mathrm{i}\left(\gamma_{\mathrm{eg}} - \gamma_{\mathrm{fe}}\right)}{(\Omega_3 - (\varepsilon_{\mathrm{f}} - \varepsilon_1) + \mathrm{i}\gamma_{\mathrm{fe}})\left(\Omega_3 - \varepsilon_1 + \mathrm{i}\gamma_{\mathrm{eg}}\right)},
\end{aligned} \tag{19}
$$

where $\sum_{\mathrm{e,e'}} 1 = 4$ for summation over the singly excited bright states. To compare equation (18) with (19) we assume the following relations between decay rates of the density matrix elements and of the single-exciton states: $\gamma_{\mathrm{fg}} = 2\gamma_1$, $\gamma_{\mathrm{eg}} = \gamma_{\mathrm{fe}} = \gamma_1$. Then the denominators of equations (18) and (19) are identical only in the harmonic case, $\varepsilon_{\mathrm{f}} = 2\varepsilon_1$, whereby $S_{\mathrm{III}}^{\mathrm{TDHF}}(\Omega_3, \Omega_2, 0) = S_{\mathrm{III}}^{\mathrm{NEE}}(\Omega_3, \Omega_2, 0) = 0$. This shows that even for a single QD (or a system of completely decoupled QDs) the NEE and TDHF spectra are, in general, different. A similar reasoning holds for the $\boldsymbol{k}_{\mathrm{I}}$ technique, with the difference that for the harmonic case $S_{\mathrm{I}}^{\mathrm{TDHF}}(\Omega_3, 0, \Omega_1) = S_{\mathrm{I}}^{\mathrm{NEE}}(\Omega_3, 0, \Omega_1)$, but they do not vanish, due to the $\mathcal{P}G^{-1}$ term in equations (8) and (9).

To compare the $\boldsymbol{k}_{\mathrm{I}}$ and $\boldsymbol{k}_{\mathrm{III}}$ techniques we consider system W for $a = 1$, i.e., for symmetric interactions $V^{\mathrm{eh}} = V^{\mathrm{ee}} = V^{\mathrm{hh}}$. As shown above, in this case the NEE $\boldsymbol{k}_{\mathrm{III}}$ response vanishes, while $\boldsymbol{k}_{\mathrm{I}}$ does not. This important difference is easily rationalized using double-sided Feynman diagrams. We choose the following single-exciton basis $|\mathrm{e}_{\mathrm{L},\sigma}\rangle = c_{\mathrm{L},\sigma}^{\dagger}d_{\mathrm{L},\bar{\sigma}}^{\dagger}|g\rangle$ and $|\mathrm{e}_{\mathrm{R},\sigma}\rangle = c_{\mathrm{R},\sigma}^{\dagger}d_{\mathrm{R},\bar{\sigma}}^{\dagger}|g\rangle$, where L and R indicate the two dots. The remaining eigenstates are optically forbidden. The doubly excited states are $|\mathrm{e}_{\mathrm{L},\sigma}\mathrm{e}_{\mathrm{L},-\sigma}\rangle$, $|\mathrm{e}_{\mathrm{R},\sigma}\mathrm{e}_{\mathrm{R},-\sigma}\rangle$ (excitons on the same dot), and $|\mathrm{e}_{\mathrm{L},\sigma}\mathrm{e}_{\mathrm{R},\sigma'}\rangle$ (excitons on different dots), while $|\mathrm{e}_{\mathrm{L},\sigma}\mathrm{e}_{\mathrm{L},\sigma}\rangle = |\mathrm{e}_{\mathrm{R},\sigma}\mathrm{e}_{\mathrm{R},\sigma}\rangle = 0$. To calculate the energies of these states we simply sum the Coulomb interactions of electrons and holes. When the two excitons are on the same dot we obtain $\varepsilon_{\mathrm{f}_1} = -4V^{\mathrm{eh}}(0) + V^{\mathrm{ee}}(0) + V^{\mathrm{hh}}(0)$, and for $a = 1$, $\varepsilon_{\mathrm{f}_1} = -2V^{\mathrm{eh}}(0)$. In the same way, for the two excitons on different dots we obtain $\varepsilon_{\mathrm{f}_2} = \varepsilon_{\mathrm{f}_1}$. All allowed single-exciton states have energy $-V^{\mathrm{eh}}(0)$, thus the energies are harmonic.

There are three types of diagrams pertinent to $\boldsymbol{k}_{\mathrm{I}}$; excited state absorption (figures 6(a), (c)), stimulated emission (figure 6(b)) and bleaching (figure 6(d)). During the time delays t_1 and t_2, the evolution of the third-order density matrix, represented by diagram (a) is identical to (b). The same holds for (c) and (d), provided we neglect population relaxation in states $|\mathrm{e}\rangle$ and $|\mathrm{g}\rangle$. For $a = 1$ we have $\varepsilon_{\mathrm{f}} = \varepsilon_{\mathrm{e'}} + \varepsilon_{\mathrm{e}}$, and the evolutions during t_3 are identical, too. Diagrams (a) and (c) have one interaction on the *bra*, so that the sign of these contributions is opposite to the sign of (b) and (d). Thus the diagrams cancel in pairs, with one notable exception: if $\mathrm{e} = \mathrm{e'}$, diagrams (a) and (c) do not contribute to the perturbative series, because $|\mathrm{ee}\rangle = 0$, while (b) and (d) do contribute (see appendix C for details). This shows that the $\boldsymbol{k}_{\mathrm{I}}$ response for this 'harmonic' system does not vanish. The same reasoning applies to $\boldsymbol{k}_{\mathrm{II}}$.

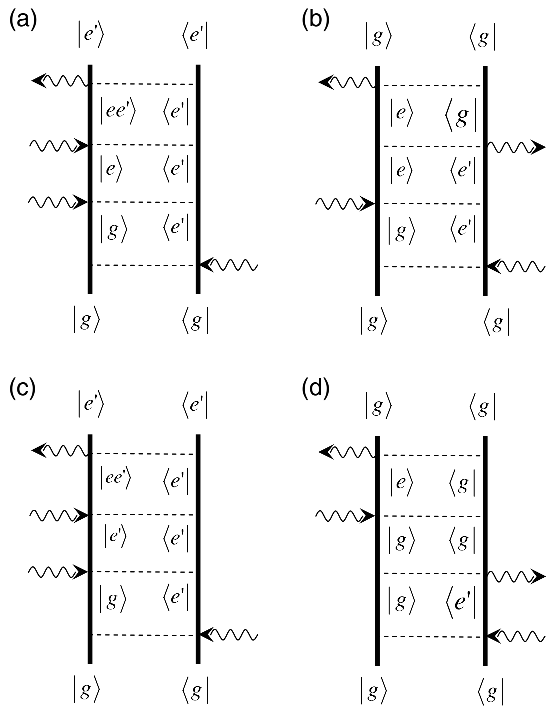

Figure 6. Double-sided Feynman diagrams for the $\boldsymbol{k}_{\mathrm{I}}$ technique. For a system with harmonic energy levels the diagrams cancel in pairs: (a) cancels (b), and (c) cancels (d) except for the $\mathrm{e} = \mathrm{e'}$ case.

We next turn to the $\boldsymbol{k}_{\mathrm{III}}$ technique (figure 7). As for $\boldsymbol{k}_{\mathrm{I}}$, the pairs of diagrams (a), (b) and (c), (d) cancel for $\mathrm{e} \neq \mathrm{e'}$. This time, however, *all four* diagrams vanish for $\mathrm{e} = \mathrm{e'}$, i.e., the $\boldsymbol{k}_{\mathrm{III}}$ signal will be zero for a 'harmonic' system, as for a system of bosons. In this sense the $\boldsymbol{k}_{\mathrm{III}}$ response is not affected by quasiparticle statistics. This sets it apart from the $\boldsymbol{k}_{\mathrm{I}}$ and the $\boldsymbol{k}_{\mathrm{II}}$ techniques.

We have used an approximate, few-parameter Hamiltonian for two identical QDs. Our Coulomb parameters agree approximately with the parameters extracted from pseudopotential calculations for an asymmetrical pair of dots [38]. These calculations predict large differences between the electron ($t^{(1)}$) and heavy-hole ($t^{(2)}$) hoppings. The TDHF and NEE spectra change in function of $t^{(2)}/t^{(1)}$, however, our main conclusion regarding the comparison between TDHF and NEE is the same.

Finally we note that the factorization formula (5) is not limited to e–h pairs and can be used for other types of

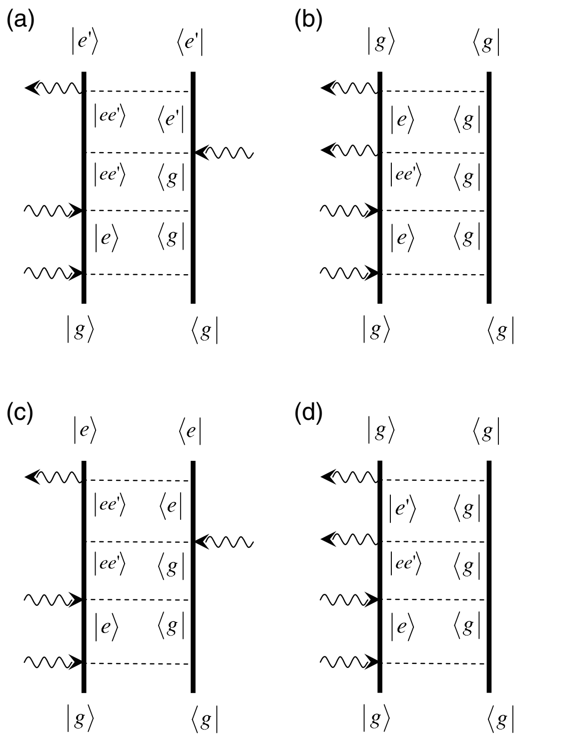

Figure 7. Double-sided Feynman diagrams for the $\boldsymbol{k}_{\mathrm{III}}$ technique. For a harmonic system the diagrams cancel in pairs: (a) cancels (b), and (c) cancels (d).

quasiparticles, such as soft and hard-core bosons (appendix A). Consequently the response functions (10)–(12) with the scattering matrix (9) can be used to describe the nonlinear optical response of molecular vibrations or Frenkel excitons in molecular aggregates

In conclusion, we have shown that the two-dimensional spectra of single and double QDs, calculated within the TDHF approach, do not properly account for the exciton–exciton interactions. These interactions play an important role in the interband nonlinear response of quantum dots. The number and positions of peaks in the TDHF spectra are at variance with results of exact (NEE) calculations. The features arising from exciton statistics, i.e., the Pauli blocking nonlinearities, are represented correctly. In the $\boldsymbol{k}_{\mathrm{III}}$ spectra these features vanish and so the response is entirely determined by Coulomb interaction nonlinearities. The $\boldsymbol{k}_{\mathrm{III}}$ technique thus clearly demonstrates the limitations of the TDHF approach.

Acknowledgments

The support of Chemical Sciences, Geosciences and Bioscience Division, Office of Basic Energy Sciences, Office of Science, US Department of Energy, is gratefully acknowledged.

Appendix A. Factorization of the Y variables

The EOM for excitations other then e–h pairs, share the same form equation (3), (see also [45]). For each type of excitation and the corresponding commutation rules, the operator $\mathcal{P}$, derived from

$$\left[\hat{B}_m, \hat{B}_n^\dagger\right] = \delta_{mn} - 2\sum_{kl} \mathcal{P}_{mknl} \hat{B}_k^\dagger \hat{B}_l, \qquad \text{(A.1)}$$

can be used to factorize the Y variables according to equation (5). For free bosons $\mathcal{P}_{mnpq} = 0$, so that $Y_{mn} = \langle B_m\rangle\langle B_n\rangle$. For hard-core bosons (Frenkel excitons) [46] the commutation operator is $\mathcal{P}_{mnpq} = \delta_{mn}\delta_{mq}\delta_{np}$ and the factorization

$$\sum_{pq} (\mathbb{I} - \mathcal{P})_{mnpq} \langle B_p\rangle\langle B_q\rangle = B_m B_n - \delta_{mn} B_m B_m,$$

is the same as for bosons, except for $\langle B_m B_m\rangle$, which must be zero for hard-core bosons.

Appendix B. Symmetrization of $\tilde{V}$

The following property of $\widetilde{V}(\mathbb{I} - \mathcal{P})$ is necessary to derive equations (10)–(12)

$$\left[\widetilde{V}(\mathbb{I} - \mathcal{P})\right]_{\mathrm{e}_4\mathrm{e}_3\mathrm{e}_2\mathrm{e}_1} = \left[\widetilde{V}(\mathbb{I} - \mathcal{P})\right]_{\mathrm{e}_4\mathrm{e}_3\mathrm{e}_1\mathrm{e}_2}.$$

From the definition (4) one can verify that $\mathcal{P}_{\mathrm{e}_4\mathrm{e}_3\mathrm{e}_2\mathrm{e}_1} = \mathcal{P}_{\mathrm{e}_4\mathrm{e}_3\mathrm{e}_1\mathrm{e}_2}$, so that only $\widetilde{V}_{\mathrm{e}_4\mathrm{e}_3\mathrm{e}_2\mathrm{e}_1} = \widetilde{V}_{\mathrm{e}_4\mathrm{e}_3\mathrm{e}_1\mathrm{e}_2}$ remains to be shown. We shall prove this in the site basis; $\widetilde{V}_{nmpq} = \widetilde{V}_{nmqp}$. The anharmonicity $\widetilde{V}$ appears in the summation $\sum_{nkl} \widetilde{V}_{mnkl} B_n^\dagger B_k B_l$, equation (6). Thus, even if $\widetilde{V}_{mnkl}$ is not symmetric in the last two indices, it can be symmetrized

$$\sum_{nkl} \widetilde{V}_{mnkl} B_n^* B_k B_l = \sum_{nkl} \tfrac{1}{2}\left(\widetilde{V}_{mnkl} + \widetilde{V}_{mnlk}\right) B_n^* B_k B_l.$$

This reasoning applies to e–h pairs as well as other types of quasiparticles discussed in appendix A.

Appendix C. Excitation statistics

Diagrams (a) and (c) in figure 6 and all diagrams in figure 7 contain the following sequence of actions on the ground state: $B_{\mathrm{e}''}B_{\mathrm{e}}^\dagger B_{\mathrm{e}'}^\dagger|g\rangle$, where e, e$'$ and e$''$ are singly excited states (we assume that $\mathrm{e} \neq \mathrm{e}'$, otherwise the diagram's contribution is zero). The diagrams have been drawn assuming

$$B_{\mathrm{e}''}B_{\mathrm{e}}^\dagger B_{\mathrm{e}'}^\dagger|g\rangle = \delta_{\mathrm{e}'\mathrm{e}''}B_{\mathrm{e}}^\dagger|g\rangle + \delta_{\mathrm{e}\mathrm{e}''}B_{\mathrm{e}'}^\dagger|g\rangle. \qquad \text{(C.1)}$$

This obviously holds for soft- and hard-core bosons. If de-excitation of $B_{\mathrm{e}}^\dagger B_{\mathrm{e}'}^\dagger|g\rangle$ leads to states other than $B_{\mathrm{e}}^\dagger|g\rangle$ or $B_{\mathrm{e}'}^\dagger|g\rangle$, then the diagrams become more complicated. We show that this does not take place for e–h pairs when using system W and the basis considered in section 5. In this case $B_{\mathrm{e}}^\dagger = c_{\mathrm{e}_1}^\dagger d_{\mathrm{e}_2}^\dagger$ (same for $B_{\mathrm{e}''}^\dagger$ and $B_{\mathrm{e}'}^\dagger$), where e_1 (e_2) indicate the electron's (hole's) position and spin projection. (We use $\mathrm{e}_{1,2}$ instead of the $m_{1,2}$ subscripts introduced in section 2, to emphasize that we deal with single-exciton *eigenstates* of the system.) From equations (A.1) and (4) we obtain

$$\begin{aligned} B_{\mathrm{e}''}B_{\mathrm{e}}^\dagger B_{\mathrm{e}'}^\dagger|g\rangle &= \delta_{\mathrm{e}'\mathrm{e}''}B_{\mathrm{e}}^\dagger|g\rangle + \delta_{\mathrm{e}\mathrm{e}''}B_{\mathrm{e}'}^\dagger|g\rangle \\ &\quad - 2\sum_{kl}\mathcal{P}_{\mathrm{e}''k\mathrm{e}l}\hat{B}_k^\dagger\hat{B}_l B_{\mathrm{e}'}^\dagger|g\rangle \\ &= \delta_{\mathrm{e}'\mathrm{e}''}B_{\mathrm{e}}^\dagger|g\rangle + \delta_{\mathrm{e}\mathrm{e}''}B_{\mathrm{e}'}^\dagger|g\rangle \\ &\quad - \delta_{\mathrm{e}''_1\mathrm{e}'_1}\delta_{\mathrm{e}''_2\mathrm{e}_2}c_{\mathrm{e}_1}^\dagger d_{\mathrm{e}'_2}^\dagger|g\rangle - \delta_{\mathrm{e}''_1\mathrm{e}_1}\delta_{\mathrm{e}''_2\mathrm{e}'_2}c_{\mathrm{e}'_1}^\dagger d_{\mathrm{e}_2}^\dagger|g\rangle. \end{aligned} \qquad \text{(C.2)}$$

The last two terms correspond to the two possibilities of annihilating the electron from one exciton and the hole from the other exciton. However, since $B_{e''}$ corresponds to an optical transition, the electron and hole it annihilates must reside on the same site and have the same spin projection. This can not be satisfied simultaneously with $e \neq e'$, given that $B_e^\dagger$ and $B_{e'}^\dagger$ correspond to optical excitations. The diagrams shown in figures 6 and 7 are thus the only ones arising for electron–hole pairs for the $\boldsymbol{k}_\mathrm{I}$ and $\boldsymbol{k}_\mathrm{III}$ techniques, under the assumption that $|f\rangle = |ee'\rangle$ and within the rotating wave approximation.

References

[1] Bryant G W and Solomon G S (ed) 2004 *Optics of Quantum Dots and Wires* (Boston, MA: Artech House publishers)

[2] Michler Peter (ed) 2004 *Single Quantum Dots: Fundamentals, Applications and New Concepts* (*Topics in Applied Physics*) 1st edn (Berlin: Springer)

[3] Grundmann M, Heinrichsdorff F, Ribbat C, Mao M-H and Bimberg D 1999 Quantum dot lasers: recent progress in theoretical understanding and demonstration of high-output-power operation *Appl. Phys.* B **69** 413–6

[4] Klimov V I, Mikhailovsky A A, Xu Su, Malko A, Hollingsworth J A, Leatherdale C A, Eisler H-J and Bawendi M G 2000 Optical gain and stimulated emission in nanocrystal quantum dots *Science* **290** 314–7

[5] Wu Y, Li X, Steel D, Gammon D and Sham L J 2004 Coherent optical control of semiconductor quantum dots for quantum information processing *Physica* E **25** 242–8

[6] Lovett B W, Reina J H, Nazir A, Andrew G and Briggs D 2003 Optical schemes for quantum computation in quantum dot molecules *Phys. Rev.* B **68** 205319

[7] Michalet X, Pinaud F F, Bentolila L A, Tsay J M, Doose S, Li J J, Sundaresan G, Wu A M, Gambhir S S and Weiss S 2005 Quantum dots for live cells, *in vivo* imaging, and diagnostics *Science* **307** 538–44

[8] Paul Alivisatos A, Gu W and Larabell C 2005 Quantum dots as cellular probes *Annu. Rev. Biomed. Eng.* **7** 55–76

[9] Stangl J, Holy V and Bauer G 2004 Structural properties of self-organized semiconductor nanostructures *Rev. Mod. Phys.* **76** 725

[10] Bayer M, Hawrylak P, Hinzer K, Fafard S, Korkusinski M, Wasilewski Z R, Stern O and Forchel A 2001 Coupling and entangling of quantum states in quantum dot molecules *Science* **291** 451–3

[11] Klimov V I 2007 Spectral and dynamical properties of multiexcitons in semiconductor nanocrystals *Annu. Rev. Phys. Chem.* **58** 635–73

[12] Gregory D S and Rumbles G 2006 Excitons in nanoscale systems *Nat. Mater.* **5** 683–96

[13] Skolnick M S and Mowbray D J 2004 Self-assembled semiconductor quantum dots: fundamental physics and device applications *Annu. Rev. Mater. Res.* **34** 181–218

[14] Haug H and Koch S W 2004 *Quantum Theory of the Optical and Electronic Properties of Semiconductors* 4th edn (Singapore: World Scientific)

[15] Chemla D S and Shah J 2001 Many-body and correlation effects in semiconductors *Nature* **411** 549–57

[16] Mukamel S 2000 Multidimensional femtosecond correlation spectroscopies of electronic and vibrational excitations *Annu. Rev. Phys. Chem.* **51** 691–729

[17] Jonas David M 2003 Two-dimensional femtosecond spectroscopy *Annu. Rev. Phys. Chem.* **54** 425–63

[18] Mukamel S and Abramavicius D 2004 Many-body approaches for simulating coherent nonlinear spectroscopies of electronic and vibrational excitons *Chem. Rev.* **104** 2073

[19] Iwaki L K and Dlott D D 2000 Three-dimensional spectroscopy of vibrational energy relaxation in liquid methanol *J. Phys. Chem.* A **104** 9101–12

[20] Tian P, Keusters D, Suzaki Y and Warren W S 2003 Femtosecond phase-coherent two-dimensional spectroscopy *Science* **300** 1553–5

[21] Zigmantas D, Read E L, Mancal T, Brixner T, Gardiner A T, Cogdell R J and Fleming G R 2006 Two-dimensional electronic spectroscopy of the B800–B820 light-harvesting complex *Proc. Natl Acad. Sci.* **103** 12672–7

[22] Borca C N, Zhang T, Li X and Cundiff S T 2005 Optical two-dimensional Fourier transform spectroscopy of semiconductors *Chem. Phys. Lett.* **416** 311–5

[23] Li X, Zhang T, Borca C N and Cundiff S T 2006 Many-body interactions in semiconductors probed by optical two-dimensional Fourier transform spectroscopy *Phys. Rev. Lett.* **96** 057406

[24] Yang L, Schweigert I V, Cundiff S T and Mukamel S 2007 Two-dimensional optical spectroscopy of excitons in semiconductor quantum wells; Liouville-space pathway analysis *Phys. Rev.* B **75** 125302 (*Preprint* cond-mat/0701424)

[25] Langbein W and Patton B 2007 Transient coherent nonlinear spectroscopy of single quantum dots *J. Phys.: Condens. Matter* **19** 295203

[26] Meier T, Thomas P and Koch S W 2006 *Coherent Semiconductor Optics: From Basic Concepts to Nanostructure Applications* 1st edn (Berlin: Springer)

[27] Mukamel S 1994 Many-body effects in nonlinear susceptibilities: beyond the local-field approximation *Molecular Nonlinear Optics, Materials, Physics, and Devices* ed J Zyss (Amsterdam: Elsevier)

[28] Kuhn O and Mukamel S 1997 Probing the two-exciton manifold of light-harvesting antenna complexes using femtosecond four-wave mixing *J. Phys. Chem.* B **101** 809–16

[29] Sieh C, Meier T, Jahnke F, Knorr A, Koch S W, Brick P, Hübner M, Ell C, Prineas J, Khitrova G and Gibbs H M 1999 Coulomb memory signatures in the excitonic optical stark effect *Phys. Rev. Lett.* **82** 3112–5

[30] Abramavicius D and Mukamel S 2005 Time-domain chirally-sensitive three-pulse coherent probes of vibrational excitons in proteins *Chem. Phys.* **318** 50–70

[31] Mukamel S, Oszwaldowski R and Abramavicius D 2007 Sum-over-states versus quasiparticle pictures of coherent correlation spectroscopy of excitons in semiconductors: femtosecond analogs of multidimensional nmr *Phys. Rev.* B **75** 245305

[32] Chernyak V, Zhang W M and Mukamel S 1998 Multidimensional femtosecond spectroscopies of molecular aggregates and semiconductor nanostructures: the nonlinear exciton equations *J. Chem. Phys.* **109** 9587–601

[33] Axt V M and Mukamel S 1998 Nonlinear optics of semiconductor and molecular nanostructures; a common perspective *Rev. Mod. Phys.* **70** 145–74

[34] Spano F C and Mukamel S 1991 Cooperative nonlinear optical response of molecular aggregates: crossover to bulk behavior *Phys. Rev. Lett.* **66** 1197–200

[35] Schweigert I V and Mukamel S 2007 Simulating multidimensional optical wave mixing signals with finite pulse envelopes *Phys. Rev.* A submitted

[36] Chernyak V, Wang N and Mukamel S 1995 Four-wave mixing and luminescence of confined excitons in molecular aggregates and nanostructures. many-body Green function approach *Phys. Rep.* **263** 213–321

[37] Kuhn O, Chernyak V and Mukamel S 1996 Two-exciton spectroscopy of photosynthetic antenna complexes: collective oscillator analysis *J. Chem. Phys.* **105** 8586
[38] Bester G, Shumway J and Zunger A 2004 Theory of excitonic spectra and entanglement engineering in dot molecules *Phys. Rev. Lett.* **93** 047401
[39] Meier F and Zakharchenya B P (ed) 1984 *Optical Orientation* (Amsterdam: North-Holland)
[40] Korkusinski M, Hawrylak P, Bayer M, Ortner G, Forchel A, Fafard S and Wasilewski Z 2002 Entangled states of electron–hole complex in a single InAs/GaAs coupled quantum dot molecule *Physica* E **13** 610–5
[41] Bayer M, Stern O, Hawrylak P, Fafard S and Forchel A 2000 Hidden symmetries in the energy levels of excitonic/'artificial atoms/' *Nature* **405** 923–6
[42] Hawrylak P 2003 Hidden symmetry and correlated states of electrons and holes in quantum dots *Solid State Commun.* **127** 793–8
[43] Piryatinski A, Ivanov S A, Tretiak S and Klimov V I 2007 Effect of quantum and dielectric confinement on the exciton–exciton interaction energy in type ii core/shell semiconductor nanocrystals *Nano Lett.* **7** 108–15
[44] Mukamel S, Oszwałdowski R and Yang L 2007 A coherent nonlinear optical signal induced by electron correlations *J. Chem. Phys.* **127** 221105
[45] Chernyak V and Mukamel S 1996 Third-order optical response of intermediate excitons with fractional nonlinear statistics *J. Opt. Soc. Am.* B **13** 1302–7
[46] Leegwater J A and Mukamel S 1992 Exciton-scattering mechanism for enhanced nonlinear response of molecular nanostructures *Phys. Rev.* A **46** 452